Theory of reconstructive phase transitions between SiO_2 polymorphs

V. P. Dmitriev
Faculty of Physics, Rostov State University, 344090, Rostov on Don, Russia

P. Tolédano
Department of Physics, University of Amiens, 33 rue Saint-Leu, 80039 Amiens, France

V. I. Torgashev
Faculty of Physics, Rostov State University, 344090, Rostov on Don, Russia

E. K. H. Salje
Department of Earth Sciences, University of Cambridge, Cambridge CB2 3EQ, United Kingdom

(Received 8 May 1998; revised manuscript received 27 July 1998)

The ordered structures of SiO_2 are shown to derive from a common parent disordered bcc structure having different fractional concentrations of SiO_2 molecules. This property allows us to describe the mechanisms of the quartz-coesite and coesite-stishovite reconstructive phase transitions, and the structure of the corresponding interphase boundaries. [S0163-1829(98)04842-5]

I. INTRODUCTION

The main crystalline forms of SiO_2 found in the earth's crust (quartz, tridymite, and cristobalite) have quite distinct structures, each with a well defined range of stability under equilibrium conditions.[1] In addition to these common SiO_2 minerals, there are at least four high pressure phases[2] (keatite, coesite, stishovite, and a hexagonal Fe_2N-type) which are also important in the crystal chemistry of the earth, in the region from the upper mantle to the lower mantle. Although the structures of all the ordered, stable and metastable, phases of SiO_2 are well known,[3] there has been no attempt to describe comprehensively the structural relationships between the various structure types, in the framework of the current theories of phase transitions. This is due to the complexity of the phase diagram of SiO_2, shown in Fig. 1, and the observations that several of the transformations between the phases are of the reconstructive type.[4] The aim of this article is twofold. At first we will show that the whole set of SiO_2 structure types can be understood within the same unified approach. More precisely, we will describe the crystal structures of silica as the result of ordering and displacive mechanisms from a parent disordered body centered cubic (bcc) structure possessing different fractional occupancies of SiO_2 molecules. This description, given in Sec. II, extends a preliminary version of our approach proposed in Ref. 5.

Another purpose of this article is to deduce from the preceding consideration the mechanisms of the reconstructive transitions between some of the SiO_2 polymorphs. In Sec. III we will describe the quartz-coesite and coesite-stishovite transformation mechanisms, and the structure of the corresponding phase boundaries. This will bring us to discuss the form of the domain walls which can be inferred from the remarkable twinning laws governing the quartz structure.

II. bcc PARENT STRUCTURE FOR THE SiO_2 POLYMORPHS

A. Crystallographic description

Let us start from the stishovite high-pressure form of SiO_2, which is stable in a wide range of pressures above 80 kbars.[6] In its rutile-type structure (space-group D_{4h}^{14}, $Z=2$) represented in Fig. 2, the Si atoms occupy the corners and center [positions 2(a)] of the tetragonal unit cell. The oxygens have an octahedral coordination[7] and lie on the diagonals of the faces perpendicular to the c axis. This corresponds to a slightly deformed bcc lattice shown in Fig. 2, one stishovite unit cell being formed by four bcc unit cells, with the following relationship between the basic translations:

$$\mathbf{a}_{st}=\mathbf{a}_1+\mathbf{a}_2+2\mathbf{a}_3, \quad \mathbf{b}_{st}=\mathbf{a}_1-\mathbf{a}_2, \quad \mathbf{c}_{st}=\mathbf{a}_1+\mathbf{a}_2, \qquad (1)$$

where $\mathbf{a}_1$, $\mathbf{a}_2$, and $\mathbf{a}_3$ are the primitive bcc lattice vectors.

In the bcc sublattice the oxygens are ordered whereas the Si atoms are randomly distributed in octahedrally coordinated positions 3(b), one site among six being filled. Therefore, one can describe the stishovite structure as the result of a hypothetical phase transition from a partially disordered bcc structure. The corresponding transition mechanism involves an ordering of the silicons in positions 2(a), while the 4(f) and 4(c) tetragonal positions remain vacant. Correlatively the oxygens are shifted in the [110] and [1$\bar{1}$0] tetragonal directions by about $0.08|\mathbf{a}_{st}|=0.33$ Å. as shown in Fig. 3.

The same bcc parent structure which has been used to deduce the stishovite structure will now be shown to constitute *the maximal substructure common to all the* SiO_2 *polymorphs provided different occupancies of the* bcc *lattice by the oxygen atoms are assumed*. Accordingly it will be used for describing successively the coesite, quartz, tridymite, cristobalite, $CaCl_2$ type and α-PbO_2 columbite-type forms of SiO_2.

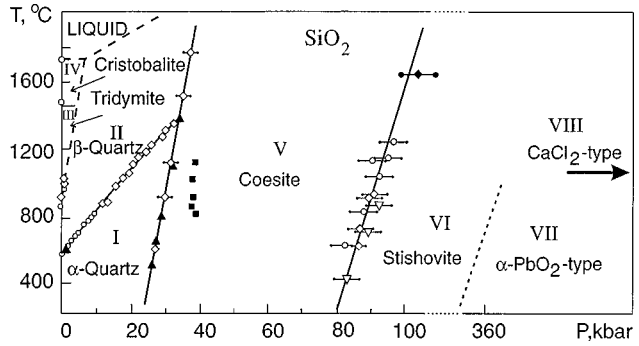

FIG. 1. Pressure-temperature phase diagram of SiO_2 from Refs. 4 and 19.

1. Coesite

The embedding of the bcc unit cell within the monoclinic structure of coesite,[8] (C_{2h}^6, $Z=16$) is shown in Fig. 4. In this unit cell the oxygens occupy randomly 2 among 3 of the 1(a) positions, whereas the Si atoms fill 1 among 9 of the 3(b) positions. Two independent mechanisms are needed to realize the coesite structure starting from a bcc structure: (1) ordering of both the O and Si atoms, which leads to a sixfold rhombohedral unit cell having the lattice parameters $\mathbf{a}_r=\mathbf{a}_1-\mathbf{a}_2$, $\mathbf{b}_r=-\mathbf{a}_1+\mathbf{a}_3$, $\mathbf{c}_r=2(\mathbf{a}_1+\mathbf{a}_2+\mathbf{a}_3)$ and (ii) displacements of some of the oxygen positions with the rhombohedral unit-cell parameters

$$\mathbf{a}_{\mathrm{coe}}=2(\mathbf{a}_1-\mathbf{a}_2),\quad \mathbf{b}_{\mathrm{coe}}=2(-\mathbf{a}_1+\mathbf{a}_3),$$

$$\mathbf{c}_{\mathrm{coe}}=4(\mathbf{a}_1+\mathbf{a}_2+\mathbf{a}_3). \tag{2}$$

In this mechanism the oxygens in monoclinic position 4(a) are unshifted, while those in positions 8(f) are shifted along the [111] bcc direction by about 0.15 Å. The remaining oxygens, in positions 4(e) and 8(f) are displaced along the diagonals of the bcc cube by ~1.25 Å.

2. β quartz

The same occupancy (2/3) of the bcc lattice by oxygen in coesite is found in the β-quartz structure[3] (D_6^4, $Z=3$) as shown in Fig. 5. Here the combined ordering and displacive mechanism associated with the virtual bcc–β-quartz transition can be more simply formulated starting from a fcc structure, formed by hexagonal close packed layers, which is obtained by a Bain deformation of the bcc unit cell.[9] It consists in a shear strain $(2e_{zz}-e_{xx}-e_{yy})$ which stretches the bcc unit cell along one of the fourfold axis and compresses it by the same extent along the other fourfold axis.[10] The correspondence between the bcc, fcc, and quartz unit cells is shown in Figs. 5 and 6(a). The relationship between the β quartz and bcc primitive translations is

$$\mathbf{a}_q=-(\mathbf{a}_2+2\mathbf{a}_3),\quad b_q=2\mathbf{a}_2+\mathbf{a}_3,\quad \mathbf{c}_q=3\mathbf{a}_1+\mathbf{a}_2+2\mathbf{a}_3. \tag{3}$$

The preceding figures show the ordering mechanism which brings the oxygen atoms in positions 2(e), the vacancies keeping the 1(a) positions, it leads to an orthorhombic structure (D_{2h}^{25}, $Z=3$) which involves a threefold multiplication of the bcc unit cell with $\mathbf{a}_{\mathrm{orth}}=\mathbf{a}_1^f+\mathbf{a}_3^f$, $\mathbf{b}_{\mathrm{orth}}=-(\mathbf{a}_2^f+\mathbf{a}_3^f)$, $\mathbf{c}_{\mathrm{orth}}=2\mathbf{a}_1^f+\mathbf{a}_2^f+2\mathbf{a}_3^f$, where $\mathbf{a}_1^f$, $\mathbf{a}_2^f$, and $\mathbf{a}_3^f$ are the fcc lattice vectors. The β-quartz structure [Figs. 6(b) and 7] results from an additional displacement of the oxygens along the diagonals of the fcc unit cell by about 0.42 Å.

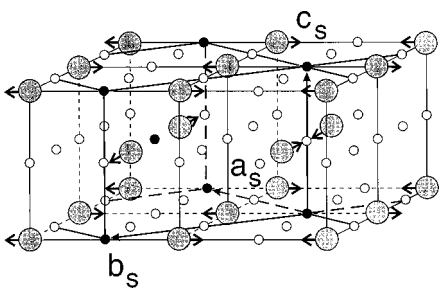

FIG. 2. Stishovite rutile-type structure (thick lines) embedded in four conventional bcc unit cells. Large grey circles are oxygens. Full and open small circles are silicons and vacancies, respectively. The arrows denote the oxygens displacements along the [110] and [$\bar{1}$10] cubic directions.

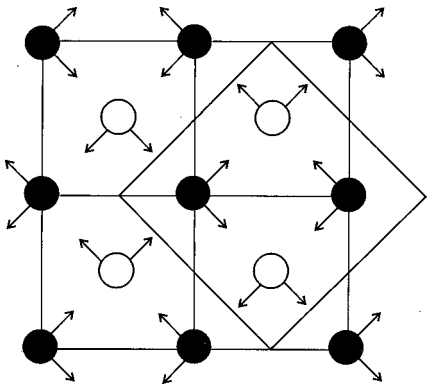

FIG. 3. Shifting of the oxygen atoms in the (001) bcc plane at the bcc-stishovite transition. Full and open circles represent oxygens located at $z=0$ and $z=1/2$. The arrows symbolize the displacements associated with the two effective order-parameter components.

3. Tridymite

The occupancy of the bcc lattice associated with the tridymite structure[10] (D_{6h}^4, $Z=4$) is $\frac{1}{2}$ since one has one

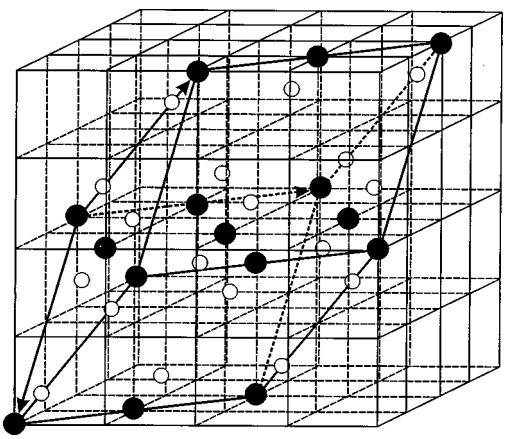

FIG. 4. bcc unit-cell (thick lines) within the coesite structure. Full and open circles are oxygens in positions 4(a) and 8(f), respectively.

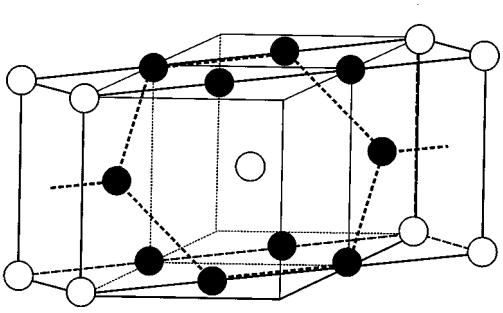

FIG. 5. Deformed hexagonal planes of β quartz within the orthorhomic configuration obtained in the bcc–β-quartz mechanism. Thin lines represent the fcc structure. Full and open circles are oxygens and vacancies, respectively.

oxygen for two sites in position 1(a) and 1 silicon for 6 sites in position 3(b) (Fig. 8). The bcc-tridymite transition mechanism can be decomposed into two steps: An ordering mechanism which brings the oxygens in positions 2(c) and 6(g), and the silicons in positions 4(f). The resulting ordered structure corresponds to an in-layer rhombohedral configuration represented in Fig. 8. In this figure, the black atoms represent oxygens and the grey atoms figure a mixture of vacancies and oxygens. The formation of the tridymite structure requires an additional Burgers-type mechanism[11] which orders the grey atoms, and shifts in the antiparallel $\pm[110]$ directions the atoms belonging to one among two (110) planes. The tridymite structure is obtained for the specific shifts of magnitude $a\sqrt{2}/12 \simeq 0.34$ Å, for which the in-layer atomic configuration becomes hexagonal (Fig. 9). The connection between the tridymite and bcc unit cells is

$$\mathbf{a}_{\mathrm{tr}}=2\mathbf{a}_1, \quad \mathbf{b}_{\mathrm{tr}}=2\mathbf{a}_2, \quad \mathbf{c}_{\mathrm{tr}}=2(\mathbf{a}_1+\mathbf{a}_2+\mathbf{a}_3). \tag{4}$$

It corresponds to a sixfold multiplication of the bcc unit cell.

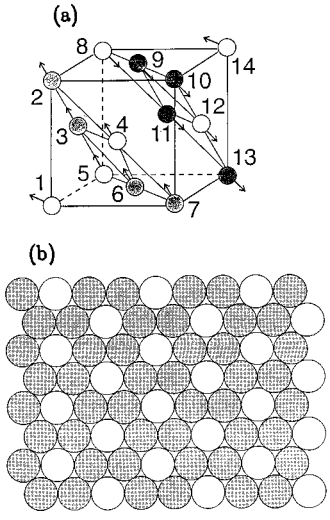

FIG. 6. (a) Ordered Bain-deformed bcc structure which transforms into β quartz after the shifts (arrows). (b) Atomic configurations within the (III) fcc plane for the Bain-deformed cubic structure and $(001)_{\mathrm{hex}}$ plane for β quartz. Grey and open circles are oxygens and vacancies, respectively.

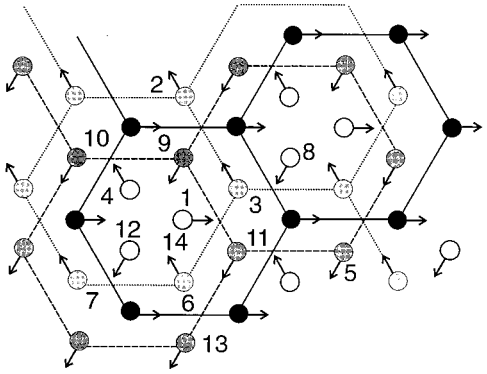

FIG. 7. Projection of the three-layered β-quartz structure on the $(0\bar{1}2)_{\mathrm{bcc}} \| (001)_{\mathrm{hex}}$ planes. Black, dark grey, and clear grey circles are oxygens at $z=0$, 1/3, and 2/3, respectively. Open circles are vacancies. The arrows show the displacement field giving rise to β quartz.

4. β cristobalite

The ideal β-cristobalite structure[12] (O_h^7, $Z=2$) and the underlying bcc lattice, which is filled by 1/2 oxygen, are shown in Fig. 10. The connection between the corresponding unit cells is

$$\mathbf{a}_{\mathrm{cr}}^{\beta}=2(\mathbf{a}_1+\mathbf{a}_2), \quad \mathbf{b}_{\mathrm{cr}}^{\beta}=2(\mathbf{a}_1-\mathbf{a}_2), \quad \mathbf{c}_{\mathrm{cr}}^{\beta}=2\mathbf{a}_3. \tag{5}$$

The mechanism of the bcc–β-cristobalite virtual transition consists essentially in an ordering process, which brings the oxygens in 4(c) and 4(d) positions. It results in a tetragonal structure (D_{4h}^{19}, $Z=2$) which is transformed in ideal β cristobalite by a Bain-type deformation, i.e., a decompression along the *c*-tetragonal axis, and a compression along the perpendicular twofold axes. This deformation[9] brings the oxygens in the fcc positions 4(c) whereas the Si atoms are distributed within SiO_4 tetrahedra according to the ''diamond law,'' i.e., they are in positions 2(a). A ''nonideal'' tetragonal structure (D_{2d}^{12}, $Z=2$) was proposed for β cristobalite,[13] which can be simply deduced from the fcc structure type, by displacing the oxygens from the 4(c) to the 4(d) positions,

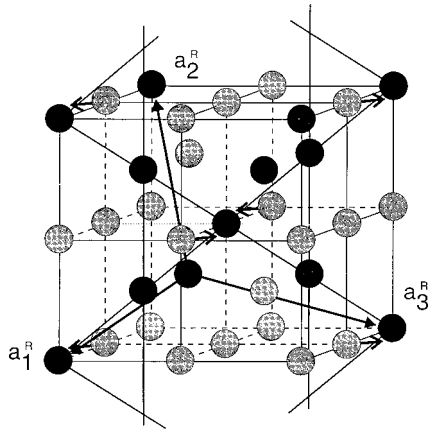

FIG. 8. Connection between the bcc conventional cell (thin lines) and the rhombohedral atomic configuration taking place at the bcc-tridymite transition mechanism. Short arrows symbolize the atomic shifts along $\pm[110]$ which yield the tridymite structure. The long arrows are the basic vectors of the rhombohedral unit cell. Full and grey circles are a mixture of oxygens and vacancies (see text).

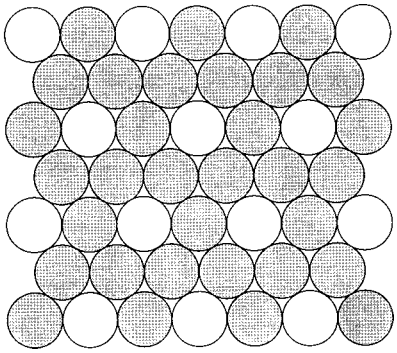

FIG. 9. Atomic configuration within the $(001)_{hex}$ plane for tridymite. Grey and open circles are oxygens and vacancies.

the Si atoms keeping their 2(a) positions. In the same way the α-cristobalite structure (D_4^4, $Z=4$) can also be directly deduced from the structure of β cristobalite, by a tilting of the SiO_4 tetrahedra, which brings the oxygens from the positions 4(c) and 8(b) and the silicons from 2(a) to 4(a). The connection between the α and β unit cells is given by

$$\mathbf{a}_{cr}^{\alpha}=\mathbf{c}_{cr}^{\beta},\quad \mathbf{b}_{cr}^{\alpha}=\mathbf{a}_{cr}^{\beta},\quad \mathbf{a}_{cr}^{\alpha}=\mathbf{a}_{cr}^{\beta}+\mathbf{b}_{cr}^{\beta}-\mathbf{c}_{cr}^{\beta}.$$

5. $CaCl_2$-type SiO_2

The othorhombic form of SiO_2 (D_{2h}^{12}, $Z=2$), which has been obtained using a 350 kbars shock wave,[14] corresponds to a slight distortion of the stishovite structure, with the oxygen displaced in general positions in the (x,y) plane, with unequal displacements in Fig. 3.

6. α-PbO_2-type SiO_2

The α-PbO_2-columbite type SiO_2 (D_{2h}^{14}, $Z=4$) was synthesized by Liu *et al.*[15] at pressures greater than 350 kbar and temperatures greater than 1000 °C. The connection between its hexagonal-deformed FeN-type unit cell[16] and the bcc structure assumed in our approach is shown in Fig. 11. The relationship between the orthorhombic and bcc lattice vectors is

$$\mathbf{a}_{col}=\mathbf{a}_1+\mathbf{a}_2+\mathbf{a}_3,\quad \mathbf{b}_{col}=2(\mathbf{a}_1+\mathbf{a}_2),\quad \mathbf{c}_{col}=-\mathbf{a}_1+\mathbf{a}_2. \tag{6}$$

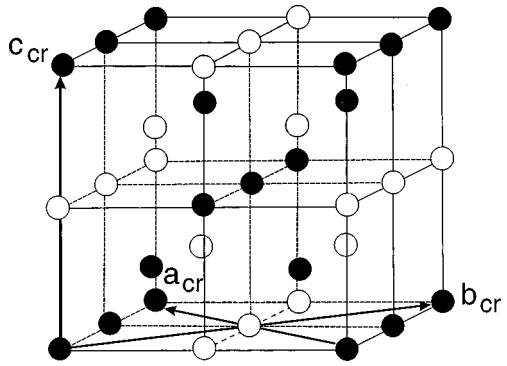

FIG. 10. Basic vectors of the β-cristobalite unit cell within the bcc lattice, before the Bain-type deformation. Full and open circles are oxygens and vacancies.

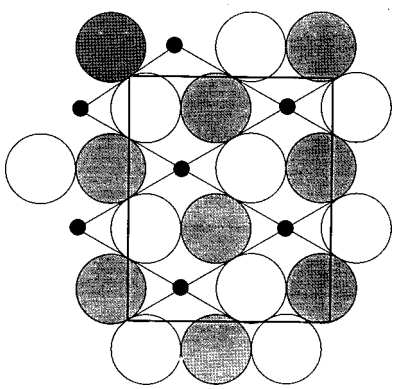

FIG. 11. Connection between the α-PbO_2 and hexagonal unit cells.

At the virtual bcc–α-PbO_2 transition the oxygens, which are fully ordered in the bcc structure, reach the 8(d) positions. The silicons, which are initially disordered in 3(b) octahedral interstitials, order in 4(c) positions. This ordering process corresponds to two combined mechanisms: (i) a Burgers-type mechanism[11,17] consisting of an antiparallel displacement of the oxygens along the [110] and [1$\bar{1}$0] bcc directions, which produces a hexagonal arrangement of the oxygens within the (110) bcc planes; (ii) an ordering of the Si atoms in 2(a) hexagonal positions.

B. Symmetry-breaking order parameters and secondary strains

In this section we determine the symmetry of the order parameters associated with the mechanisms proposed for the virtual bcc-SiO_2 polymorphs transitions. We also calculate the lattice parameters resulting from the transition mechanisms. By comparison with the experimental parameters we evaluate the magnitude of the secondary (improper) strains which must be taken into account to obtain the experimental numbers in a quantitative model. Such strains provide useful indications on the character (strong or weak) of the reconstructive transitions *between* the SiO_2 polymorphs, which are described in Sec. III. In the following considerations we use Kovalev's notation[18] for the wave vectors expressed in function of the reciprocal bcc lattice vectors

$$\mathbf{a}_1^*=\left(O,\frac{2\pi}{a},\frac{2\pi}{a}\right),\quad \mathbf{a}_2^*=\left(\frac{2\pi}{a},O,\frac{2\pi}{a}\right),$$

$$\mathbf{a}_3^*=\left(\frac{2\pi}{a},\frac{2\pi}{a}O\right).$$

Kovalev's notation is also used for the labeling of the irreducible representations (IR's) which determine the order-parameter symmetries. The relevant points of the bcc Brillouin-zone (BZ) involved in the preceding symmetries are indicated in Fig. 12. The standard theoretical procedure [11] used to determine the order-parameter symmetries is recalled in the Appendix.

1. The bcc-stishovite transition

The breaking of the translational symmetry expressed by Eq. (1) corresponds to the wave vectors $\mathbf{k}_9=\frac{1}{2}(\mathbf{a}_1^*+\mathbf{a}_2^*)$, lo-

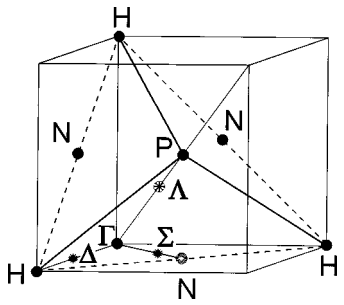

FIG. 12. Points and lines of the bcc Brillouin zone involved in the transition mechanisms from the bcc structure to the SiO_2 structures.

cated at the N point of the bcc BZ surface. The star of $\mathbf{k}_9$ has six branches,[18] and therefore the IR $\tau_4(\mathbf{k}_9)$ associated with the bcc-stishovite transition is six-dimensional. The equilibrium values of the corresponding six-component order parameter are $(\eta, -\eta, 0,0,0,0)$, i.e., the tetragonal stishovite symmetry is determined by two effective nonvanishing components of the order parameter. Assuming a cubic lattice parameter of $a=2.9$ Å, which coincides with the best fit with respect to the different SiO_2 structures as deduced from our approach, the transition mechanism yields the calculated stishovite unit-cell parameters: $a_{\rm st}^c=4.1$ Å and $c_{\rm st}^c=2.9$ Å. Compared with the experimental values[19] ($a_{\rm st}^{\rm ex}=4.179$ Å, $c_{\rm st}^{\rm ex}=2.665$ Å) it implies taking into account an additional compression along z of about 2% and a decompression along x and y of $\simeq 8\%$.

2. bcc coesite

The combined ordering and displacive mechanisms associated with bcc-coesite transition requires two distinct, eight and six-dimensional IR's of the O_h^9 space group: $\tau_1(\mathbf{k}_7) \oplus \tau_4(\mathbf{k}_9)$ where $\mathbf{k}_7=\frac{1}{6}(\mathbf{a}_1^*+\mathbf{a}_2^*+\mathbf{a}_3^*)$ is located inside the bcc BZ along the Λ line (Fig. 12). The equilibrium values of the corresponding coupled order parameters are respectively, $(\eta,0,0,0,\eta,0,0,0)$ and $(0,\xi,0,0,0,0)$. The calculated lattice parameters resulting from the assumed transition mechanism are $a_{\rm coe}^c=b_{\rm coe}^c=8.2$ Å, $c_{\rm coe}^c=10.05$ Å, and $\gamma=120°$. The difference with the experimental numbers[8] ($a_{\rm coe}^{\rm ex}=b_{\rm coe}^{\rm ex}=7.17$ Å, $c_{\rm coe}^{\rm ex}=12.38$ Å) is large, since one needs compressions of about 13% along a, b and c.

3. bcc-β quartz

The complex ordering and displacive mechanisms described in Sec. II A for the bcc–β-quartz transition have the symmetry of the reducible representation $\tau_1(\mathbf{k}_8)\oplus\tau_4(\mathbf{k}_4)$ where $\mathbf{k}_8=\frac{1}{3}(\mathbf{a}_1^*+\mathbf{a}_2^*+\mathbf{a}_3^*)$ and $\mathbf{k}_4=\frac{1}{3}\mathbf{a}_3^*$ corresponds, respectively, to the Λ and Σ lines of the bcc BZ. The equilibrium values of the six-component order parameter transforming as $\tau_1(\mathbf{k}_8)$ are $(\eta,0,0,\varepsilon^*\eta,0,0)$, where $\varepsilon^*=e^{2i\Pi/3}$. The effective components of the twelve-dimensional order parameter related to $\tau_4(\mathbf{k}_4)$ are $(\eta,-\eta,0,0,0,0,0,0,0,0,0,0)$. The calculated values found for the β-quartz unit-cell parameters are $a_q^c=4.81$ Å. and $c_q^c=6.48$ Å. With respect to the experimental values[3] ($a_q^{\rm ex}=5.45$ Å, $c_q^{\rm ex}=4.99$ Å) it implies considering a large compression of about 30% along the y axis and an analogous decompression along z.

4. bcc tridymite

The sixfold multiplication of the bcc unit cell, expressed by Eq. (4), which characterizes the bcc-tridymite transition, corresponds to two IR's of the O_h^9 space group: a six-dimensional IR $[\tau_1(\mathbf{k}_9)]$ associated with the first step ordering mechanism described in Sec. II A, with the equilibrium order parameter values $(0,\eta,0,-\eta,0,-\eta)$, and a twelve dimensional IR ($\tau_4(\mathbf{k}_4)$) reflecting the second step (ordering and displacements) of the Burgers-type mechanism leading to the tridymite structure, with an order-parameter symmetry $(\eta,-\eta,0,0,0,0,0,0,0,0,0,0)$. The calculated lattice parameters are $a_{\rm tr}^c=5.023$ Å and $c_{\rm tr}^c=8.20$ Å. These values are close to the experimental numbers[10] ($a_{\rm tr}^{\rm ex}=5.03$ Å, $c_{\rm tr}^{\rm ex}=8.22$ Å), i.e., no substantial additional deformation is needed for the transition.

5. bcc-β cristobalite

The bcc–β-cristobalite transition involves the same six-dimensional IR $\tau_1(\mathbf{k}_9)$ as the bcc tridymite and bcc-coesite transitions, but with a different set of equilibrium values of the order-parameter components $(0,0,-\eta,\eta,\eta,\eta)$. The calculated lattice parameters are $a_{\rm cr}^c=b_{\rm cr}^c=8.2$ Å and $c_{\rm cr}^c=5.8$ Å which compared to the experimental values[12] ($a_{\rm cr}^{\rm ex}=7.05$ Å) require to take into account the ''reversed'' Bain deformation mechanism restoring the fcc cristobalite structure (see Sec. II A). This deformation[9,11] involves a compression along a and b of about 13% and a decompression along c of $\sim+21\%$. The tetragonal structure proposed for β cristobalite is induced by the three-dimensional zone-center (IR) ($(\tau_8(\mathbf{k}_{11}))$ of the O_h^7 space group. Another IR of $O_h^7[\tau_4(\mathbf{k}_{10})]$ allows us to describe the β-α cristobalite transition, where $\mathbf{k}_{10}$ coincides with the X-point of the fcc BZ surface.

6. bcc-$CaCl_2$-type SiO_2

Although the $CaCl_2$-type structure of SiO_2 can be simply obtained from the stishovite parent structure at a zone-center IR $[\tau_5(\mathbf{k}_{17})]$ of the tetragonal BZ, which is commonly involved in rutile-type structures, one can also describe this structure as resulting directly from the bcc structure. The same IR $[\tau_4(\mathbf{k}_9)]$ associated with the bcc-stishovite transition, leads to $CaCl_2$-SiO_2 but for different equilibrium values of the six-component order parameter $(\eta_1,\eta_2,0,0,0,0)$. The calculated lattice parameters ($a_{\rm cacl}^c=4.06$ Å, $b_{\rm cacl}^c=2.9$ Å) differ substantially from the experimental values[14] ($a_{\rm cacl}^{\rm ex}=4.09$ Å, $c_{\rm cacl}^{\rm ex}=4.50$ Å, $b_{\rm cacl}^{\rm ex}=3.79$ Å) and require us to consider the improper strains: $e_1=e_2=7.3\%$, $e_3=-17.9\%$, $e_6=8.8\%$.

7. bcc-α-PbO_2-type SiO_2

The mechanism involved in the bcc-α-PbO_2 type SiO_2 transition is associated with the same IR $\tau_4(\mathbf{k}_9)$ than the bcc-stishovite transition. The additional ordering of the Si atoms in hexagonal positions corresponds to the $\tau_2(\mathbf{k}_8)$ IR with the following equilibrium values of the six-component order-parameters $(\eta,0,0,\eta,0,0)$. The calculated orthorhombic lattice parameters are $a_{\rm Pb}^c=c_{\rm Pb}^c=4.06$ Å and $b_{\rm Pb}^c=5.8$ Å, which compared to the experimental values[15,16] ($a_{\rm Pb}^{\rm ex}$

TABLE I. Symmetry of the order parameters associated with the ordering and displacive mechanisms, transforming the bcc parent structure into the SiO_2 structures. Columns (2), (3), and (4) give (i) the irreducible representations corresponding to the ordering [column (2)] and displacive [columns (3) and (4)] mechanisms, in Kovalev's notation (Ref. 18), and in the international notation of the points and lines of the bcc Brillouin zone. (ii) The equilibrium values of the order-parameter components. Note that the Bain deformation, which transforms as the zone-center (Γ) two-dimensional representation Eg is indicated for β quartz and β cristobalite but not for coesite where it is not a symmetry breaking deformation.

(1) SiO_2 polymorphs	(2) Ordering	(3) Displacement	(4) Additional displacement
Stishovite			
	$\tau_4(\mathbf{k}_9)(N_4)$		
	$(\eta\ \eta\ 0\ 0\ 0\ 0)$		
Coesite	$\tau_4(\mathbf{k}_9)(N_4)$	$\tau_1(\mathbf{k}_7)(\Lambda_1)$	
	$(0\ \eta\ 0\ 0\ 0\ 0)$	$(\eta\ 0\ 0\ 0\ \eta\ 0\ 0\ 0)$	
β quartz			
	$\tau_1(\mathbf{k}_8)(\Delta_1)$	$\tau_3(\mathbf{k}_{11})(\Gamma,\mathrm{Eg})$	$\tau_4(\mathbf{k}_4)(\Sigma_4)$
	$[\eta\ 0\ 0\ (\varepsilon^*\eta)0\ 0]$	$(\eta\ 0)$	$(\eta\ -\eta\ 0\ 0\ 0\ 0\ 0\ 0\ 0\ 0\ 0)$
Trydimite			
	$\tau_1(\mathbf{k}_9)(N_1)$	$\tau_4(\mathbf{k}_4)(\Sigma_4)$	
	$(0\ \eta\ 0\ -\eta\ 0\ -\eta)$	$(\eta - \eta\ 0\ 0\ 0\ 0\ 0\ 0\ 0\ 0\ 0)$	
β cristobalite			
	$\tau_1(\mathbf{k}_9)(N_1)$	$\tau_3(\mathbf{k}_{11})(\Gamma,\mathrm{Eg})$	
	$(0\ 0\ -\ \eta\ \eta\ \eta\ \eta)$	$(\eta\ 0)$	
$CaCl_2$ type			
	$\tau_4(\mathbf{k}_9)(N_4)$		
	$(\eta_1\ \eta_2\ 0\ 0\ 0\ 0)$		
α-PbO_2 type			
	$\tau_4(\mathbf{k}_9)(N_4)$	$\tau_2(\mathbf{k}_8)(\Delta_2)$	
	$(\eta\ \eta\ 0\ 0\ 0\ 0)$	$(\eta\ 0\ 0\ \eta\ 0\ 0)$	

$=4.181$ Å, $c^c_{\mathrm{Pb}}=3.842$ Å, and $b^c_{\mathrm{Pb}}=4.617$ Å) require compressions along x, y, and z ($e_1=e_2=2.9\%$, $e_3=17.9\%$) and decompression along the x,y direction ($e_6=-4.4\%$).

C. Density and degree of occupancy of the bcc structure

Tables I and II summarize respectively, the order-parameter symmetries and strain values which are involved in the virtual transitions from the bcc parent structure to the various SiO_2 structure types. The magnitude of the improper strains indicated in Table II are only a rough estimate since we have assumed the same bcc unit-cell parameter ($a=2.9$ Å) for all the SiO_2 structures without considering the increase of hydrostatic compression with increasing pressure. The large deformations needed for a quantitative agreement with the experimental lattice parameters for β quartz and β cristobalite actually correspond to the standard values found for the Bain deformation in alloys.[9,11] For coesite the required deformation reflects the strongly reconstructive character of the stishovite-coesite transformation (see Sec. III).

Figure 13 depicts the connections, assumed in our approach, between the SiO_2 polymorphs and their common virtual parent structure. The possibility of a high pressure bcc configuration of SiO_2 molecules has been already suggested by a numbers of authors,[20,21] as representing the closest SiO_2 packing which may be obtained when increasing the pressure. It also represents the most realistic configuration that can be assumed for SiO_2 close packed clusters (at variance with hcp of fcc packings) which may form within the melt when approaching solidification. A bcc cluster realises in the simplest way the tetrahedral and octahedral distributions of chemical bonds which constitute the basic motifs in SiO_2 polymorphs.

It is shown in Fig. 13 that there is a simple connection between pressure P, density ρ, and the degree of occupancy x of the bcc structure by oxygen atoms, and the correlated influence of these parameters on the structural changes in

TABLE II. Magnitude of the secondary deformations (strain components) which have to be taken into account in order to obtain a coincidence between the calculated and experimental values of the lattice parameters. + and − denote a decompression and a compression, respectively.

SiO_2 polymorphs	$e_{xx}=e_1$	$e_{yy}=e_2$	$e_{zz}=e_3$	$e_{yz}=e_4$	$e_{xz}=e_5$	$e_{xy}=e_6$
Stishovite	0.08	0.08	−0.02			
Coesite	−0.127	−0.127	−0.127	0.131	0.131	0.131
β quartz		−0.345	0.31	0.038		
Tridymite	0.062	0.062	−0.133			0.037
β cristobalite	−0.128	−0.128	0.213			
$CaCl_2$ type	0.073	0.073	−0.179			0.088
α-PbO_2 type	−0.029	−0.029	−0.179			0.044

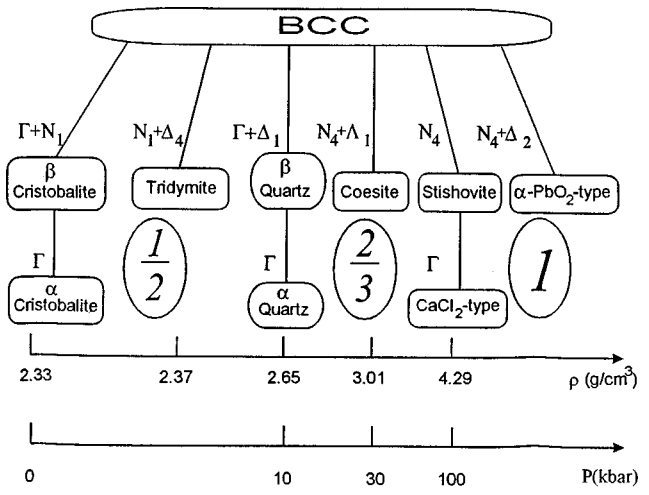

FIG. 13. Connection between the bcc parent structure and the SiO_2 polymorphs described in the present work. The points of the bcc Brillouin zone involved in the virtual transition mechanisms are indicated by the current Greek symbols, as well as the respective occupancies of the bcc unit cell (circled numbers). The densities and pressures corresponding to each structure are given at the bottom of the figure.

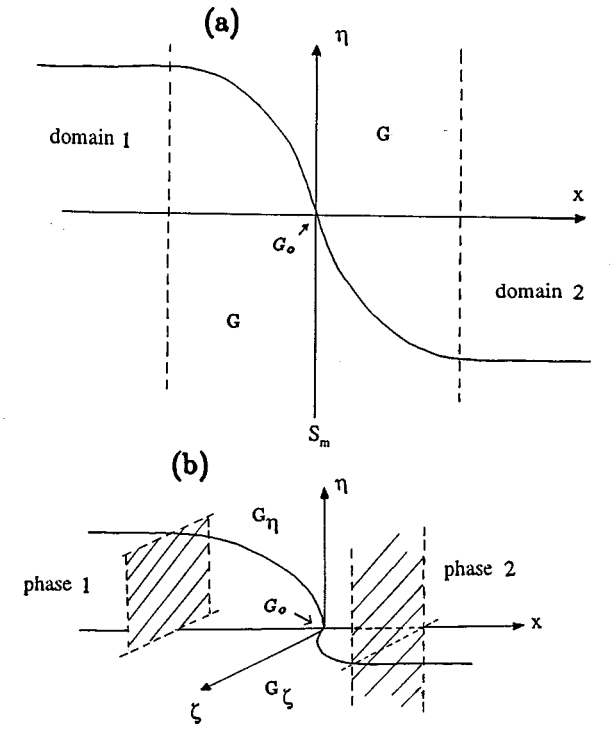

FIG. 14. (a) Variation of the order-parameter magnitude across a domain wall in the case of a single order-parameter component (see text). (b) Variation of the order-parameter magnitude across the interphase between two phases associated with different order-parameters η and ζ from a common parent phase (see text).

SiO_2. For the lowest pressure phases (cristobalite, tridymite) one has the lower density of ~ 2.35 g/cm^3 and the minimal degree of occupancy $x=\frac{1}{2}$. When increasing pressure by a few kbars but below about 80 kbars the density increases to 2.65–3 g/cm^3 and the degree of occupancy jumps to $x=\frac{2}{3}$. For pressure above 80 kbars, the density reaches its highest values of ~ 4.3 g/cm^3 and one has a maximal occupancy of $x=1$ for the oxygens in the parent structure. This close correlation between P, ρ, and x denotes an implicit morphotropic character for the sequence of reconstructive transitions which take place along the P-axis: tridymite $\rightarrow$cristobalite$\rightarrow$quartz$\rightarrow$coesite$\rightarrow$stishovite$\rightarrow\ldots$, i.e., the degree of occupancy x of the bcc structure plays the role of concentration in open systems such as solid solutions.

III. RECONSTRUCTIVE PHASE TRANSITIONS BETWEEN SiO_2 POLYMORPHS

In this section we describe the mechanisms which can be deduced from our approach for the quartz-coesite and coesite-stishovite transformations and the subsequent features of the corresponding interphase boundaries. Before, we will briefly recall the formalism currently used[22] for describing interphases or twin boundaries, and underline some specific symmetry properties of the interphases at reconstructive phase transitions.

A. Preliminary considerations

Let us consider a transition between two phases, denoted 1 and 2, which are structurally distorted with respect to a common parent phase, denoted O. If (e_{ij}) and (e'_{ij}) are the set of spontaneous strain components associated with the deformations of phase 1 and 2, respectively, then, following the notation of Metrat,[22] one can define the components of the distortion tensors $(M_{ij})=E+(e_{ij})$ and $(N_{ij})=E+(e'_{ij})$, where E is the second rank unity tensor. The tensor (D_{ij}) whose elements are $D_{ij}=\Sigma_{k=l}(N_{ij}N_{jk}-M_{ik}M_{jk})$ allows us to write under the simple forms

$$\sum_{i,j} x_i x_j D_{ij}=0 \tag{7}$$

the equations providing the geometry of the phase boundary between phase 1 and 2. In Eq. (7), x_i and x_j are the space coordinates. Defining the invariants $I=t_r(D_{ij})$, $D=\det(D_{ij})$, and $J=(D_{11}D_{22}-D_{12}^2)+(D_{22}D_{33}-D_{23}^2)+(D_{33}D_{11}-D_{13}^2)$, one can show[23] that among the solutions of Eq. (7) figure the two following cases: (1) $D\neq 0$, and DI and J are of opposed sign. In this case the phase boundary has the form of a conical surface.[23] (2) $D=0$ and $J<0$: the phase boundary corresponds to a couple of intersecting planes.

If one assumes a *thick* phase boundary between phases 1 and 2, i.e., not reduced to one or two layers, there exists a surface S_m inside the phase boundary, which corresponds to a minimal deformation. Different situations can be described with respect to the symmetry of the phase boundary and of the surface S_m, depending on the dimensionality and symmetry of the order parameters describing the $O\rightarrow 1$ and $O\rightarrow 2$ phase transitions. (i) Let us first examine the situation where phases 1 and 2 are two different orientational domains of the same phase, connected by a group–subgroup relationship to the symmetry of the parent phase O. If the order parameter associated with the $O\rightarrow 1$ (or $O\rightarrow 2$) transition has only one component η, then the volume limiting the phase boundary has the symmetry of phase 1 (and 2) and is symmetric with respect to S_m. Figure 14(a) shows that η

$=0$ on the surface S_m, whose symmetry corresponds to a cross section of the parent phase O. If one deals with a multicomponent order parameter each domain may correspond to a set of different equilibrium values of the order-parameter components, therefore the interphase region may display a symmetry different from the symmetry of phases 1 and 2. For example, a parent phase of cubic symmetry may give rise to orientational domains of symmetry D_{3d} corresponding to the equilibrium values of three order-parameter components: (η,η,η) and $(\eta,-\eta,-\eta)$. In this case the interphase has a different symmetry (e.g., tetragonal) associated with the equilibrium values $(\eta, 0\ 0)$ of the order-parameter components. The symmetry of the surface S_m is also tetragonal, and coincides with a cross section of the tetragonally distorted cubic phase.

(ii) Another situation occurs if phases 1 and 2 are different phases associated with different order parameters from the parent phase. When their symmetries correspond to (different) subgroups of the parent symmetry, then the interphase will be asymmetric, and the volumes on each side of S_m have the respective symmetries of phase 1 and 2, as shown in Fig. 14(b). At the surface S_m, one shifts from one to another set of order-parameter components in such a way that the symmetry of S_m coincides again with the symmetry of a cross section of the parent phase. If phases 1 and 2 are not group/subgroup related to phase O, then the symmetries of the interphase, on each side of S_m, will be the intersection of the symmetries of phases 1 and 2 with the symmetry of the parent phase, respectively. This latter situation is realized at the β-quartz-coesite interphase boundary which is described in the following section.

B. The β-quartz-coesite reconstructive transition

From the analysis of the β-quartz and coesite structures presented in Secs. II A and II B, one can infer the following mechanisms for the β-quartz-coesite transformation.[24–26] Both structures have the same occupancy of the bcc unit cell ($x=2/3$) but display different types of orderings corresponding to distinct order-parameter symmetries [$\tau_1(\mathbf{k}_8)$ for β quartz and $\tau_1(\mathbf{k}_7)$ for coesite]. It implies that the reordering mechanism from one to the other structures requires *diffusion*, i.e., the quartz-coesite transformation should exhibit a sluggish kinetics.

After the ordering process, the oxygen ions in β quartz are organized in specific hexagonal planes, perpendicular to the six fold axis of the β-quartz structure. The three consecutive planes which form the three-layered quartz structure are shifted in directions forming angles of 120°. Within the coesite structure the atoms located in the preceding planes are displaced in different directions in such a way that no regular dense plane remains in the coesite structure.

Table II shows that there is a change in the sign of the deformation with respect to the bcc structure along the z axis, from 0.31 in β quartz to -0.127 in coesite. Correlatively the deformation e_2 decreases from -0.345 to 0.127. The relative volume per mol decreases from $V_{\rm mol}^{\rm quartz}=22.69\ {\rm cm}^3/{\rm mol}$ to $V_{\rm mol}^{\rm coes}=20.64\ {\rm cm}^3/{\rm mol}$ which denotes a moderate reconstructive character. This conclusion is supported by the values of the jumps in enthalpy and entropy found experimentally.[25] $\Delta H\simeq 320$ cal/mol and $\Delta S=-1.2$ cal/kmol.

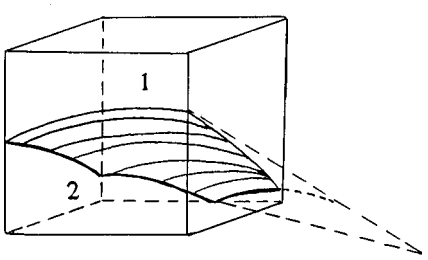

FIG. 15. Cone-type surface separating two interphase regions.

Using the formalism developed in Sec. III A and the values of the strains given in Table II, one can calculate the second-rank distortion tensors (M_{ij}) and (N_{ij}) for β quartz and coesite, which yield the values of the (D_{ij}) tensor components:

$$(D_{ij})\equiv\begin{pmatrix} -0.21 & 0.25 & 0.25 \\ 0.25 & 0.35 & 0.17 \\ 0.25 & 0.17 & 0.93 \end{pmatrix}. \tag{8}$$

It gives $D=0.13$, $I=-0.79$, and $J=-0.36$. Hence $D\neq 0$, $DI<0$ and $J<0$. The phase boundary between the two phases is limited by conical surfaces, as shown in Fig. 15.

The symmetries of β quartz and coesite do not correspond to subgroups of O_h^9 (see Sec. II A). Therefore the phase boundary between the two phases should be asymmetric, and display a different symmetry in the region adjacent to each phase. One finds that the symmetry of the phase boundary should be monoclinic C_2 close to the β-quartz phase and monoclinic C_{2h} close to the coesite phase. The intermediate region of the interphase surrounding the S_m plane should possess a higher (orthorhombic) symmetry corresponding to a Bain-deformed cross section of the parent bcc phase.

C. The coesite-stishovite reconstructive transition

From coesite to stishovite the occupancy of the bcc structure changes from $x=\frac{2}{3}$ to $x=1$. The corresponding reordering of the silicons bring all the atoms to their bcc positions. Thus, in contrast with the quartz-coesite transformation which requires a limited diffusion within each unit cell, the coesite-stishovite transformation mechanism implies a large-scale diffusion process which empties part $(\frac{1}{3})$ of the bcc unit cells and fills $\frac{2}{3}$ of the remaining unit cells. The important increase in density at this transformation reflects its diffusive nature and its strongly reconstructive character, which is attested by the large value found for the enthalpy:[27] $\Delta H\approx 1170$ cal/mol, although the entropy jump is moderate: $\Delta S\approx -1$ cal/kmol. Note that the resulting stishovite structure is practically free from deformation with respect to the assumed bcc structure, since the strain components reduce to 2% for e_3 and 8% for e_1 and e_2, as shown in Table II.

Using the numbers given in Table II one finds for the distortion tensors

$$(M_{ij})_{\rm coes}=\begin{pmatrix} 0.873 & 0.131 & 0.131 \\ 0.131 & 0.873 & 0.131 \\ 0.131 & 0.131 & 0.873 \end{pmatrix},$$

$$(N_{ij})_{\text{stich}}=\begin{pmatrix}1.0800\\ 01.080\\ 0.00.98\end{pmatrix}. \tag{9}$$

One can see that the nondiagonal distortion components vanish at the coesite-stishovite transformation, whereas the diagonal components exhibit a small jump. From Eq. (9) one can deduce the (D_{ij}) tensor:

$$(D_{ij})=\begin{pmatrix}0.4 & -0.246 & -0.246\\ -0.246 & 0.4 & -0.246\\ -0.246 & -0.246 & 0.146\end{pmatrix}, \tag{10}$$

which yields $D=-0.062$, $I=0.964$, and $J=0.11$. Hence the coesite-stishovite phase boundary is limited by cone-type surfaces shown in Fig. 15. The region adjacent to coesite has again the monoclinic point-group C_{2h}. On the other hand the stishovite structure coincides with a subgroup of $O_h^9(D_{4h}^{14})$ and therefore the region of the phase boundary adjacent to the stishovite phase has a tetragonal symmetry D_{4h}. The surface S_m dividing the asymmetric coesite-stishovite phase boundary corresponds to a shifting from the bcc-coesite $[\tau_1(k_7)]$ to the bcc-stishovite $[\tau_4(k_9)]$ order parameters, namely from the equilibrium values $(\eta\,0\,0\,0\,0\,0)$ to $(\eta\,-\eta\,0\,0\,0\,0)$ of the order-parameter component. Thus, the atoms are shifted, with respect to the cubic positions, according to the nonzero order-parameter components $(\eta\,0\,0\,0\,0\,0)$. Taking into account the change in concentration $(\frac{2}{3}\rightarrow 1)$ and the difference of the distortion tensors (10), one can conclude that the phase boundary between coesite and stishovite should display and inhomogeneous structure, i.e., its lattice should be macroscopically distorted and its structure disordered.

D. The Japanese twins of quartz

An indication in favor of a parent bcc structure for quartz can be found in the existence of the so-called Japanese twins, observed in β and α-quartz.[3] Following our description of the bcc–β-quartz transition, the orientation of the sixfold axes in β quartz should correspond to cubic directions such as [120] and [012] [Fig. 16(a)] which transform one into another by the cubic C_4^x axis, and to the direction [201] obtained by a fourfold rotation C_4^z. Furthermore, the structure of the domain walls separating Japanese twins should reflect the structure of the parent bcc phase, i.e., it should correspond to a Bain-deformed section of the bcc structure having on average a planar orthorhombic symmetry.

The calculated values of the strain tensor components given in Table II for β quartz allow to deduce the distortion tensors for two Japanese twins oriented along [021] (domain 1 and [012] (domain 2). One finds

$$(M_{ij})^1=\begin{pmatrix}1 & 0 & 0\\ 0 & 0.655 & 0.0385\\ 0 & 0.0385 & 1.31\end{pmatrix},$$

$$(N_{ij})^2=\begin{pmatrix}1 & 0 & 0\\ 0 & 1.31 & -0.0385\\ 0 & -0.0385 & 0.655\end{pmatrix}, \tag{11}$$

which yield

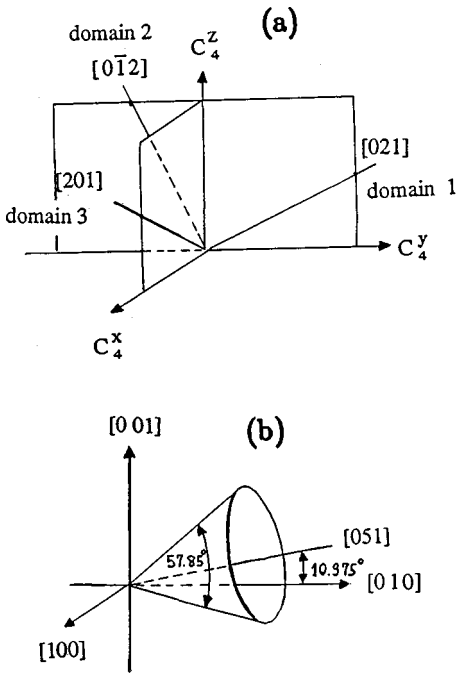

FIG. 16. (a) Orientational domains corresponding to the cubic directions [021] (domain 1), [012] (domain 2), and [201] (domain 3). (b) Geometrical parameters of the conical domain wall between the domains 3 and 1.

$$(D_{ij})=\begin{pmatrix}0 & 0 & 0\\ 0 & 1.287 & -0.151\\ 0 & -0.151 & -1.287\end{pmatrix} \tag{12}$$

corresponding to $D=0$, $I=0$, and $J=-1.679$, therefore the domain wall between the domains 1 and 2 is formed by two intersecting planes. Let us note that the domain 3 corresponding to the cubic direction [201] in Fig. 16(a) is associated with a distortion tensor with respect to, let say, the domain 1:

$$(D_{ij})=\begin{pmatrix}0.43 & 0 & 0.076\\ 0 & -0.45 & -0.88\\ 0.076 & 0.027 & 1.66\end{pmatrix}. \tag{13}$$

Therefore one finds $D=-0.31$, $I=1.64$, $J=-0.256$, i.e., the form of the domain wall 3-1 (as well as 3-2) *will not be planar but conical*, the axis of the cone being oriented along the [051] cubic direction, as shown in Fig. 16(b).

To determine the structure of the domain wall between the domains 1 and 2, one can refer to the mechanism proposed in Sec. II for the bcc–β-quartz transition. This mechanism involves two distinct, twelve and six-dimensional, order parameters having the symmetries $\tau_3(\mathbf{k}_4)$ and $\tau_1(\mathbf{k}_8)$, respectively. The twelve-dimensional order parameter undergoes at the middle surface S_m a cross-over from the equilibrium values $(\eta-\eta\,00\,00\,00\,00\,00)$ to $(00\,00\,00\,00-\eta\eta\,00)$ when going from one to the other domain. Therefore, it vanishes on S_m and does not affect the form of this surface. By contrast the six-dimensional order parameter goes from the value $(\eta\,00(\varepsilon^*\eta)00)$ to $((\varepsilon\eta)\eta\,00\;\eta\,0)$. Hence on the S_m surface, η_1 and η_4 exhibit a jump of $\pm(\eta-\varepsilon^*\eta)$. Consequently S_m will have the symmetry of a *tetragonal* cross section of the parent bcc structure, corresponding to the equi-

librium values of the order parameter $[(\eta-\varepsilon^*\eta)\ 00\ (\varepsilon^*\eta-\eta)\ 00]$. It means that on the S_m surface the distortion component M_{yz} changes its sign, whereas M_{yy} and M_{zz} exhibit jumps of $\pm(\eta_1-\eta_4)$ without changing sign. Accordingly, the S_m surface, as well as the domain wall between the domains 1 and 2, should be deformed along the *y* and *z* axes.

IV. SUMMARY AND CONCLUSION

In summary, it has been shown that the whole set of stable structures pertaining to the pressure-temperature phase diagram of SiO_2 can be deduced from a common bcc parent structure, through ordering and displacive mechanisms. For a quantitative agreement with the experimental numbers obtained for the lattice parameters, additional secondary strains have to be taken into account. The existence of a common reference bcc structure allows to describe the mechanism of the actual reconstructive transformations between quartz and coesite, and between coesite and stishovite. It gives also the possibility to predict the form and symmetry of the phase boundaries between the preceding phases.

Such considerations lead also to a possible interpretation of the pressure-induced amorphous phase, which has been termed α-SiO_2 (Ref. 28) obtained from α quartz, coesite, and stishovite.[28,29] In contrast to the crystalline SiO_2 structures, which are shown in our model to correspond to fractional occupancies ($x=\frac{1}{2},\frac{2}{3},1$) of the bcc structure the α-SiO_2 structure may be associated with irrational values of *x*, varying continuously between the fractional numbers. This idea is supported by the linear increase in density with increasing pressure, measured in α-SiO_2,[30] and by the observation that this densification occurs with an increase of the coordination number, which varies from 4 to 6 through intermediate coordination value,[31] including a fivefold coordination.[32] In this respect it can be noted that the α-SiO_2 phase is more easily obtained from crystal structures (quartz, coesite) in which the tetrahedral coordination is deformed. Along the same line, the existence of vacancies in the bcc lattice, assumed in our model, should favor the amorphization process, since it allows an uncorrelated aggregation of SiO_2 clusters, which may lead in the intermediate region of the phase diagram ($x=\frac{2}{3}$) to the formation of microcrystals possessing differently ordered and deformed structures with respect to the parent bcc structures. Such microcrystals have been observed by electron microscopy in the amorphization process of α quartz.[33] Accordingly the α-SiO_2 phase can be interpreted as an assembly of microcrystalline regions involving different types of coordinations, which is incompatible with a crystalline order.

ACKNOWLEDGMENT

The Russian Foundation for Fundamental Research has supported this work (Grant No. 97-02-17878).

APPENDIX

In this appendix we summarize the procedure used in Sec. II B for determining the order-parameter symmetries corresponding to a given transformation from the bcc phase. As an illustrative example we consider the bcc-stishovite transition which involves the space-group change $O_h^9 \rightarrow D_{4h}^{14}$ and a fourfold multiplication of the bcc unit cell.

The connections between the basic vectors of the stishovite ($\mathbf{a}_{st},\mathbf{b}_{st},\mathbf{c}_{st}$) and bcc ($\mathbf{a}_1,\mathbf{a}_2,\mathbf{a}_3$) unit cells are given by Eq. (1) (Sec. II A). From this equation one can deduce the transition $\mathbf{k}$ vector as follows: $\mathbf{k}$ satisfies the set of equations $\exp\{i\mathbf{k}\cdot\mathbf{a}_{st}\}=\exp\{i\mathbf{k}\cdot\mathbf{b}_{st}\}=\exp\{i\mathbf{k}\cdot\mathbf{c}_{st}\}=1$, or equivalently $(\mathbf{k}\cdot\mathbf{a}_{st})=2\pi n$, $(\mathbf{k}\cdot\mathbf{b}_{st})=2\pi n$, $(\mathbf{k}\cdot\mathbf{c}_{st})=2\pi n$, where *n* is an integer. Writing $\mathbf{k}$ under the general form $\mathbf{k}=\alpha\mathbf{a}_1^*+\beta\mathbf{a}_2^*+\gamma\mathbf{a}_3^*$, where $\mathbf{a}_1^*$, $\mathbf{a}_2^*$, and $\mathbf{a}_3^*$ are the basic reciprocal bcc lattice vectors (explicited in Sec. II B), yield the system of equations: $\alpha+\beta=0,1...$; $\alpha-\beta=0,1...$; $\alpha+\beta+2\gamma=0,1...$. This system possesses only two acceptable solutions: ($\alpha=\beta=1/2$, $\gamma=0$) and ($\alpha=\beta=0$, $\gamma=1/2$), which correspond to the two wave vectors: $\mathbf{k}_1=\frac{1}{2}\mathbf{a}_3^*=(\pi/a,\pi/a,0)$ and $\mathbf{k}_2=\frac{1}{2}(\mathbf{a}_1^*+\mathbf{a}_2^*)=(\pi/a,-\pi/a,0)$. $\mathbf{k}_1$ and $\mathbf{k}_2$ are actually two *branches* of the *star* of the wave vector[11] denoted $\mathbf{k}_9^*$ in Kovalev's tables.[18] $\mathbf{k}_9^*$, which coincides with the *N*-point of the bcc Brillouin zone shown in Fig. 12, is invariant by the symmetry operations of the point group D_{2h} (*mmm*). Therefore the number of branches of $\mathbf{k}_9^*$ is given by the ratio: $[\text{Order of } O_h]/[\text{Order of } D_{2h}]=6$. The six branches of $\mathbf{k}_9^*$ have the coordinates $\mathbf{k}_9^1=(\pi/a,\pi/a,0)$, $\mathbf{k}_9^2=(\pi/a,-\pi/a,0)$, $\mathbf{k}_9^3=(\pi/a,0,\pi/a)$, $\mathbf{k}_9^4=(\pi/a,0,-\pi/a)$, $\mathbf{k}_9^5=(0,\pi/a,\pi/a)$, and $\mathbf{k}_9^6=(0,\pi/a,-\pi/a)$.

Since the point-group D_{2h} has eight one-dimensional irreducible representations (IR's), one can construct the eight six-dimensional IR's of the O_h^9 symmorphic space group associated with $\mathbf{k}_9^*$ using the standard procedure described, for example, in Refs. 11 and 18. These IR's, which are denoted $\tau_1(\mathbf{k}_9),\tau_2(\mathbf{k}_9),\ldots,\tau_8(\mathbf{k}_9)$ induce a number of symmetry groups, subgroups of O_h^9, which have been tabulated in Refs. 34 and 35. One can verify in the tables that the only IR which leads to the stishovite D_{4h}^{14} symmetry is $\tau_4(\mathbf{k}_9)$. It corresponds to the equilibrium values of the six-component order parameter: $\eta_1=-\eta_2=\eta\neq 0$, $\eta_3=\eta_4=\eta_5=\eta_6=0$, as indicated in Refs. 34 and 35.

[1] R. B. Sosman, *The Phase of Silica* (Rutgers University Press, New Brunswick, NJ, 1965).

[2] L. G. Liu, in *High Pressure Research in Geophysics*, edited by S. Akimoto and M. H. Manghnani (CAPJ, Tokyo, 1982), p. 349.

[3] L. Bragg and G. F. Claringbull, *Crystal Structures of Minerals* (Bell and Sons, London, 1965).

[4] L. Merill, J. Phys. Chem. Ref. Data **11**, 1043 (1982).

[5] V. Dmitriev, V. Torgashev, P. Toledano, and E. K. H. Salje, Europhys. Lett. **37**, 553 (1997).

[6] L. G. Liu, W. A. Bassett, and T. Takahashi, J. Geophys. Res. **79**, 1160 (1974).

[7] E. C. T. Chao, J. J. Fahey, and J. Littler, J. Geophys. Res. **67**, 419 (1962).

[8] T. Zoltai and M. J. Buerger, Z. Kristallogr. **111**, 129 (1959).

[9] E. C. Bain, Trans. AIME **70**, 25 (1924).
[10] J. E. Fleming and H. Lynton, Phys. Chem. Glasses **1**, 148 (1960).
[11] P. Tolédano and V. Dmitriev, *Reconstructive Phase Transitions* (World Scientific, Singapore, 1996), Chap. 3.
[12] R. W. G. Wyckoff, Z. Kristallogr. **62**, 189 (1925).
[13] W. Nieuwenkamp, Z. Kristallogr. **92**, 82 (1935).
[14] K. T. Park, K. Terakura, and V. Matsui, Nature (London) **336**, 670 (1988).
[15] L. G. Liu, W. A. Bassett, and J. Sharry, J. Geophys. Res. **78**, 2301 (1978).
[16] V. N. German, M. A. Podurets, and R. Trunin, Sov. Phys. JETP **37**, 107 (1973).
[17] W. G. Burgers, Physica (Amsterdam) **1**, 561 (1934).
[18] O. V. Kovalev, *Irreducible Representations of the Space Groups* (Gordon and Breach, New York, 1965).
[19] L. G. Liu and W. A. Bassett, *Elements, Oxides and Silicates* (Oxford University Press, New York, 1986), p. 110.
[20] H. Sowa, Z. Kristallogr. **184**, 257 (1988).
[21] R. H. Hazen, W. L. Finger, R. J. Hemley, and H. K. Mao, Solid State Commun. **72**, 507 (1989).
[22] G. Metrat, Ferroelectrics **26**, 81 (1980).
[23] G. A. Korn and T M Korn, *Mathematical Handbook for Scientists and Engineers* (McGraw-Hill, New York, 1965).
[24] G. MacDonald, Am. J. Sci. **254**, 713 (1956).
[25] J. S. Weaver, D. W. Chipman, and T. Takahashi, Am. Mineral. **64**, 604 (1979).
[26] P. W. Mirwald and H. F. Massonne, J. Geophys. Res. **85**, 6983 (1980).
[27] S. Akimoto and Y. Siono, J. Geophys. Res. **74**, 1653 (1969).
[28] R. J. Hemley, A. R. Jephcoat, H. K. Mao, L. C. Ming, and M. H. Manghnani, Nature (London) **334**, 52 (1988).
[29] Y. Tsuchida and T. Yagi, Nature (London) **347**, 267 (1991).
[30] J. S. Tse, D. D. Klug, and Y. Le Page, Phys. Rev. B **46**, 5933 (1992).
[31] Q. Williams, R. J. Hemley, M. B. Kruger, and R. Jeanloz, J. Geophys. Res. **98**, 157 (1993).
[32] J. Badio, J. L. Barrat, and P. Gillet, Phys. Rev. Lett. **76**, 772 (1996).
[33] K. J. Kingma, C. Meade, R. J. Hemley, K. H. Mao, and D. R. Veblen, Science **259**, 666 (1993).
[34] J. C. Tolédano and P. Tolédano, Phys. Rev. B **21**, 1139 (1980).
[35] H. T. Stokes and D. M. Hatch, *Isotropy Subgroups of the 230 Crystallographic Space Groups* (World Scientific, Singapore, 1988).